Materials Science in Semiconductor Processing 88 (2018) 167–172

Contents lists available at ScienceDirect

Materials Science in Semiconductor Processing

journal homepage: www.elsevier.com/locate/mssp

Structural and photoluminescent properties of $CuGa_xIn_{1-x}Se_2$ thin films prepared by close-spaced vapor transport technique

Houda Tassoult[a,b,c,*], Abdesselam Bouloufa[a,b], Marek Pawlowski[d], Malgorzata Igalson[d]

[a] Laboratory of Electrochemical and Materials (LEM), Ferhat Abbas-Sétif-1 University, Sétif, 19000, Algeria
[b] Electronics Department, Faculty of Technology, Ferhat Abbas-Sétif-1 University, Sétif, 19000, Algeria
[c] Unité de Développement des Equipements Solaires, UDES, Centre de Développement des Energies Renouvelables, CDER, 42004 Tipaza, Algeria
[d] Warsaw University of Technology, Faculty of Physics, Semiconductor Division, Koszykowa 75, 00-662 Warszawa, Poland

ARTICLE INFO

Keywords:
$Cu(In,Ga)Se_2$
CSVT
Photoluminescence
Raman spectroscopy
XRD

ABSTRACT

$CuGa_xIn_{1-x}Se_2$ (CIGS) (x = 0, x = 0.3 and x = 1) absorber layers were deposited onto transparent conducting oxide (SnO_2) substrates using close-spaced vapor transport technique (CSVT). The aim of this work was to assess the quality of CIGS absorber films with various gallium contents. Composition found by Energy Dispersive Spectroscopy (EDS) showed that the investigated samples were Cu-poor and $CuGa_{0.3}In_{0.7}Se_2$ thin film had a composition close to 0.3 as planned. The structural properties were investigated by X-ray diffraction analysis (XRD) and Raman spectroscopy, while optical properties were investigated by measuring transmittance and photoluminescence spectroscopy. It was found that all investigated samples crystallize with (112) as a preferential crystallographic direction. The shift of the XRD peaks towards a higher value of 2θ with the increase of Ga composition was observed. The grain size determined from the width of 112 XRD peak was within 40–75 nm range with no clear correlation with Ga content. Raman spectra of samples with x = 0 and 0.3 featured mainly a peak assigned to the A_1 mode at about 175 cm^{-1}. In $CuGaSe_2$ the secondary Cu_2Se phase was detected both by XRD and Raman. The band gap as evaluated by optical transmission measurement is shifted towards lower than expected values due to substantial defect-related bands broadening. A large concentration of defects in the samples was also confirmed by low or absent PL signal in the vicinity of the bandgap, while the emission due to deep defects was prevailing in the spectrum. The optoelectronic properties as indicated by photoluminescence have to be improved if CSVT method of absorber preparation is to be used more widely in photovoltaics.

1. Introduction

Among thin film solar cells, the $Cu(In, Ga)Se_2$-and CdTe-based ones exhibit the highest efficiency [1]. Recently, Kamada et al. [2] achieved a new world record efficiency of 22.8% for CIGS thin-film solar cells in laboratory scale cells by substituting the ZnO/CdS buffer with optimized (Zn,Mg)O/Zn(O,*S*,OH) buffer layers. The drawback of CIGS technology is rather complicated absorber preparation technology; therefore other methods are studied with the aim of finding the cheapest, possibly non-vacuum and easy to upscale fabrication method while still preserving the high efficiency of the devices. Close-spaced vapor transport (CSVT) is an easy process of thin films fabrication which is not only a technique suitable for large-scale module production but also the one with the potential to yield high module efficiencies [3–5]. However, not much work has been done up to now on CIGS absorbers obtained by CSVT technique used to investigate their properties and opto-electronic quality as a function of gallium.

The structural quality of the films might be revealed using X-ray diffraction spectroscopy and Raman spectroscopy while photoluminescence (PL) is a non-destructive tool providing insight into their optoelectronic quality in terms of concentration of defects responsible for recombination [6]. In this work, we use the above-mentioned methods for characterization of the series of $CuGa_xIn_{1-x}Se_2$ samples fabricated by CSVT method with various gallium contents: x = 0, x = 0.3 and x = 1. The main goal is to find out whether structural and opto-electronic properties of these films signify quality necessary for making them suitable as absorbers in efficient solar cells.

2. Experimental details

Samples were grown onto SnO_2 substrates using close-spaced vapor transport technique. The powder used as a material source in the CSVT

* Corresponding author at: Laboratory of Electrochemical and Materials (LEM), Ferhat Abbas-Sétif-1 University, Sétif, 19000, Algeria.
E-mail address: tassoulthouda@yahoo.fr (H. Tassoult).

https://doi.org/10.1016/j.mssp.2018.08.001
Received 2 April 2018; Received in revised form 1 August 2018; Accepted 2 August 2018

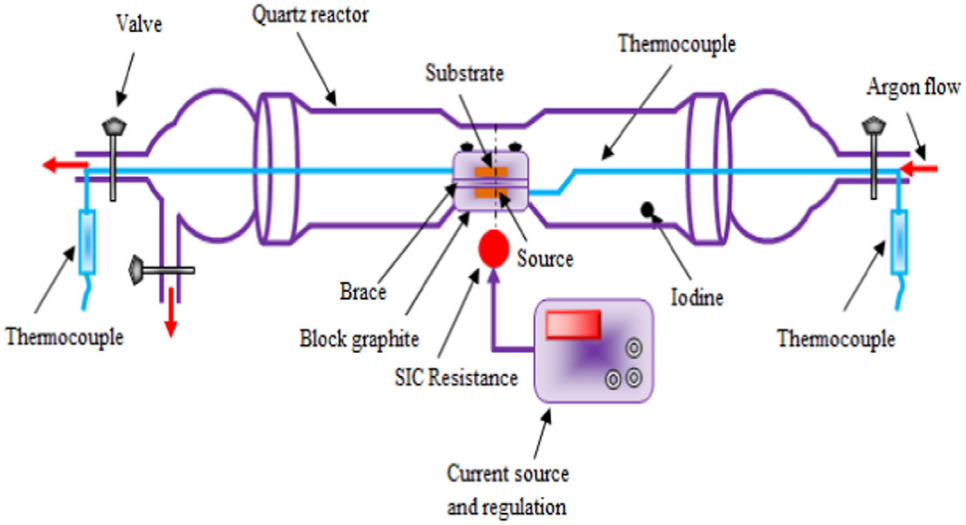

Fig. 1. Schematic of horizontal CSVT reactor system.

Table 1
EDS compositional analysis of the CIGS thin films.

Sample	Atomic compositions					
	at% Cu	at% In	at% Ga	at% Se	Ga/(Ga + In)	Cu/(In + Ga)
CIS	24.61	27.05	/	48.34	0	0.90
CIGS	27.21	19.11	8.67	45.01	0.31	0.97
CGS	26.09	/	26.86	47.05	1	0.96

system was obtained from polycrystalline CIS, CIGS and CGS ingots grown by cooling a molten stoichiometric mixture of (Cu (99.9999%), In (99.999%), Ga (99.9995%) and Se (99.999%)) elements (Alfa Aesar). The CIS, CIGS, and CGS alloy ingots were then reduced to a fine powder by optimizing the milling conditions to develop powder grain sizes less than 40 μm. After milling, the powder was compressed to form pellets by using a hydraulic press system with a pressure of about 3×10^4 kPa. Solid iodine was used as the transporting agent and it is kept in the lower-temperature region. The reaction zone consists of a graphite cell placed in a quartz reactor. The atmosphere used during the deposition was Ar-gas with few mTorr pressures, while the temperature difference between source and substrate is about 50 °C. Material is transported from the source to the substrate through iodine which acts as a transport agent. The graphite blocks are heated by SiC resistance. The temperatures of the blocks are controlled separately by thermocouples. The substrate temperatures were varied between 400 °C and 530 °C during 30 min at a growth rate of up to 250 nm/min (more details on CSVT technique can be found elsewhere [3–5,7]).

The schematic drawing of the CSVT system is shown in Fig. 1.

The EDS compositional analysis of $CuGa_xIn_{1-x}Se_2$ thin films are measured by JEOL-JSM 5310 LV scanning electron microscopy operating at an accelerating voltage of 15 kV and equipped with an energy dispersive spectroscopy (EDS) analytical system.

XRD experiments for structural analysis of these thin films were performed for 2θ configuration over 10–120° using X'pert PANalitycal Philips diffractometer, Bragg-Brentano system, (Cu-Ka radiation, λ = 1.5406 Å).

The structural characteristics of the considered samples were also investigated by Raman spectroscopy using RENISHAW in Via Raman Microscope with an Ar^+ laser excitation source of 633 nm.

The optical properties, including transmittance and reflectance, were recorded using Bentham PVE300 setup in the 300–1800 nm range of light wavelength. The reflectance was measured in the diffused standard.

The PL measurements were carried out in a temperature range of 20–200 K provided by helium closed-cycle cryostat. The incident laser light of 514.5 nm line (Ar+ blue laser) was focused on the sample's surface with a maximal power of about 100 mW/cm^2. The area of a laser spot was about 2 mm^2. The iHR550 grating monochromator was used. The PL signal was collected by a liquid nitrogen cooled germanium detector and amplified by using a standard lock-in technique (Stanford Reserach SR 530 with choppoer SR 540) [8].

3. Results and discussion

3.1. Structural analysis

The results of EDS compositional analysis of $CuGa_xIn_{1-x}Se_2$ thin films are summarized in Table 1. All films were Cu-poor and CIGS thin film had a composition close to 0.3 as planned.

To examine the crystalline phases of the films, XRD measurements were carried out. The diffraction spectra of our samples are presented in Fig. 2. Main peaks appear associated to (112), (200), (220)/(204), (221) and (312)/(116) planes of the chalcopyrite structure with (112) as the preferential crystallographic direction. This preferential orientation was located around 26.86°, 26.94° and 28.41° for CIS, CIGS, and CGS respectively. The increase of Ga led to a shift of peak position towards higher values of 2θ and this shift, as reported by Olejníček et al. [9], is consequently due to the decrease in lattice constants *a* and *c*.

The inter-plane distances (d_{hkl}) for the samples were calculated using Bragg's diffraction equation:

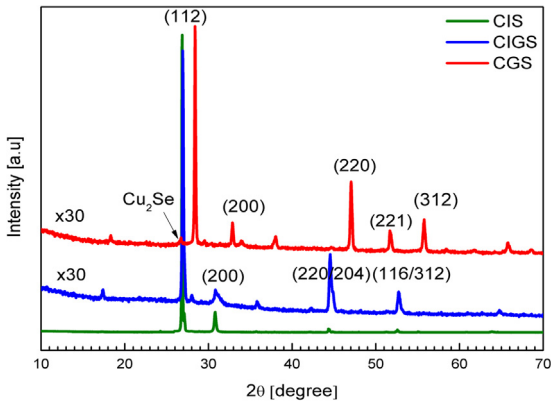

Fig. 2. XRD patterns for CIS, CIGS and CGS.

Table 2
The particle size G and inter-planar distances d of the thin films.

Peak	Samples	2θ	d_{hkl}(Å)	*FWHM* (radians)	Grain size G (nm)
[112]	CIS	26,86	3.316	0,00199	75
	CIGS	26,94	3.306	0,00371	40
	CGS	28,41	3.139	0,00307	49

$$d_{hkl} = n\lambda/2\sin\theta \quad (1)$$

where n is a positive integer, λ = 1.5406 Å and θ is the Bragg's angle.

The crystallite size G of CIGS was estimated by using Scherrer's formula

$$G = k\lambda/\beta\cos\theta \quad (2)$$

where k is a dimensionless crystallite shape factor, λ is the X-ray wavelength, β is the full width at half maximum intensity (FWHM), and θ is the Bragg angle [10–12]. The most common value for k is around 0.94.

Table 2 summarizes the average grain size G and inter-planar distances of the thin films.

For the quadratic system ($a = b \neq c$) in which the $CuGa_xIn_{1-x}Se_2$ compounds crystallize, the inter-reticular distance d_{hkl} is given by:

$$d_{hkl} = 1/\sqrt{\frac{h^2+k^2}{a^2} + \frac{l^2}{c^2}} \quad (3)$$

From the X-ray spectra, we calculated the lattice constants a and c. The values found are listed in Table 3.

As given in Table 2, the inter-planar spacing (d_{112}) decreases from 3.316 to 3.139 Å with Ga concentration increase, as expected. The lattice constant values a and c are also affected by GGI ratios as shown in Table 3 and they decrease as GGI increases. As indicated e. g. by Vidhya et al. [10] this behavior is due to a different ionic size of Ga (0.62 Å) and In (0.81 Å). We would also expect the decrease of the grain size with increasing gallium content as found in CIGS films by Claypoole et al. and Witte et al. [13,14] by combining two characterization techniques, secondary ion mass spectroscopy (SIMS) and scanning electron microscopy (SEM). In contrast here we observed that CGS sample has a slightly higher grain size than CIGS sample which probably means that the presence of In-Ga mixture has a negative impact on the grain growth in the case of *CSVT* technique.

Fig. 3 shows Raman spectrum measured on our films. The spectrum features a prevailing peak at about 175 cm^{-1} for CIS and CIGS, that is assigned to the basic A_1 mode dominating in Raman for the chalcopyrite Cu(In,Ga)Se_2 phase. A similar value was found by Izquierdo-Roca et al. (2011) [15], Fontané et al. [16], and Liu et al. [17]. According to Insignares-Cuello et al. [6], the Ga/(In + Ga) ratio play a critical role in the frequency of this peak. As Ga concentration increases, the signal shifts toward larger diffraction angle as reported by Theodoropoulou et al. [18]. Furthermore, the morphology of the chalcopyrite, in particular, the compositional structure and formation mechanism play a role in the intensity and sharpness of this peak.

As shown in Fig. 3, the 175 peak is not visible in CGS. Indeed, in this sample, other peaks than those belonging to the chalcopyrite structure were noticed. These peaks are consistent with the results reported by Ben Marai et al. [11]. Based on what Izquierdo-Roca et al. (2007) [19] reported, the additional peak observed for CGS in the range 290–320 cm^{-1} was assigned to Cu_2Se secondary phase. It is worth

Table 3
The crystalline parameters of the investigated samples.

Samples	a (Å)	c (Å)	c/a
CIS	5.76	11.40	1.97
CIGS	5.74	11.38	1.98
CGS	5.45	10.80	1.98

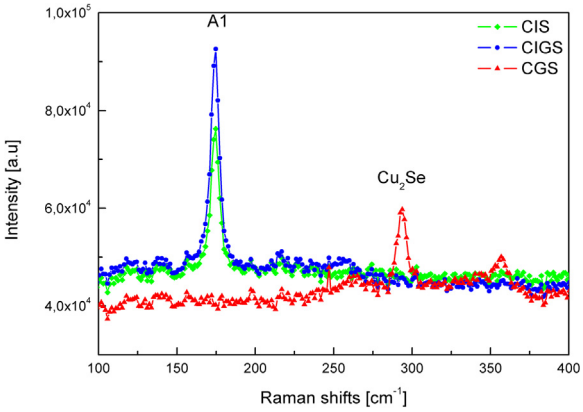

Fig. 3. Raman spectra of CIGS samples on SnO_2 substrate (with x = 0, 0.3, 1).

noticing that a close examination of the XRD patterns of CGS (see Fig. 2) reveals small peak around 26° consistent with Cu_2Se phase as reported by Ben Marai et al. [11], Cho et al. [20], and Witte et al. (2008) [21].

Summing up, the Raman spectroscopy indicated inferior CGS thin film quality comparing to other CIGS compositions.

3.2. Optical measurements

The optical properties of the CIGS thin films were studied by measuring transmittance spectra in the range 300–1800 nm. Using transmission and reflection measurements, the absorption coefficient α was calculated using the following expression:

$$\alpha = -ln(T/1-R)/d \quad (4)$$

Here d refers to the estimated thickness of the polycrystalline thin film (Our samples are roughly 2 μm thick).

Fig. 4 shows the Tauc plot of the absorption coefficient of the CIGS thin films obtained from transmission and reflection measurements. We have to add, that due to a presence of the thin back surface layer of unknown origin, the absolute values of transmission were distorted even below the bandgap they did not exceed 25% - therefore we show the $\alpha^2(h\nu)$ plot in arbitrary units. Despite that, all films feature a well-defined absorption edge in the range of 700–1300 nm. The linear extrapolation of the $(\alpha h\nu)^2$ dependence gives an estimation of the bandgap energy E_g = 0.98, 1.12 and 1.57 eV for CIS, CIGS, and CGS, respectively (Fig. 4). Values of 1.04 and 1.68 eV were found by Witte et al. [14,21] and 1.14 eV by Contreras et al. [22] for CIS, CGS, and CIGS, respectively. The shift of our results towards lower energies is expected for highly defected material. The optical bandgap of $CuGa_xIn_{1-}$

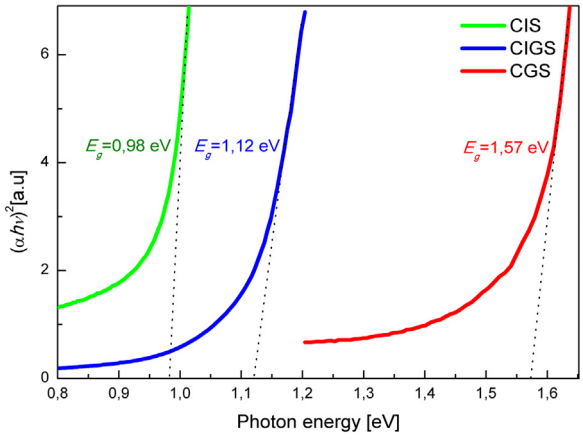

Fig. 4. Plot of $(\alpha h\nu)^2$ versus photon energy $h\nu$ of CIGS films.

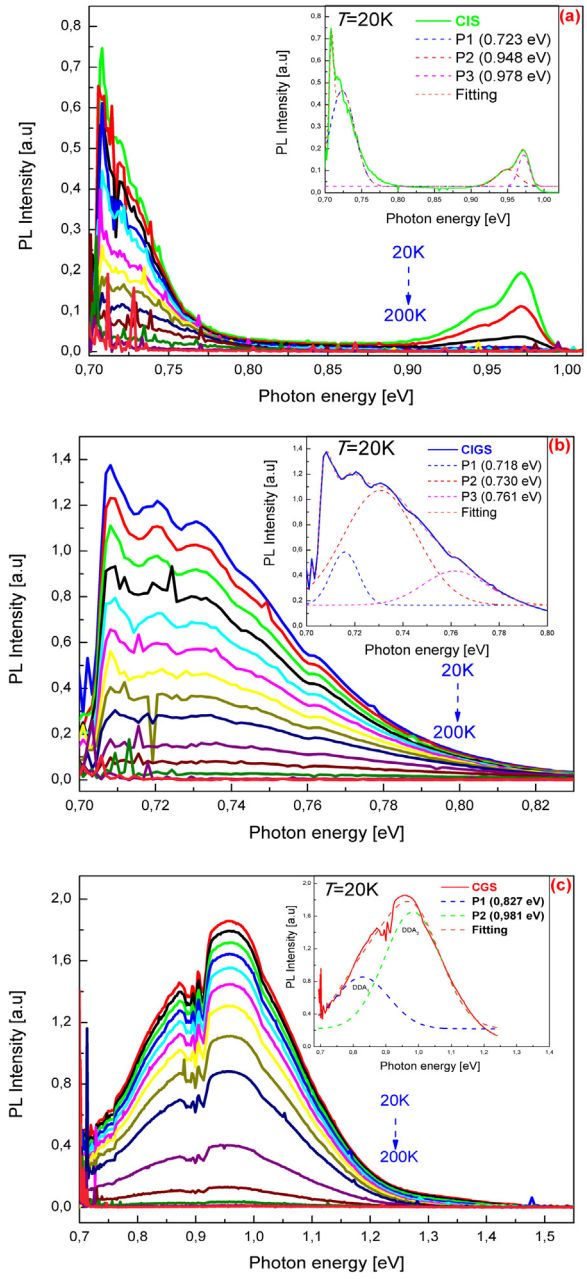

Fig. 5. PL spectra of CIGS thin films under temperature 20–200 K. Insets are the fitting result of the deep bands of PL spectrum at 20 K using Gaussian distribution.

$_xSe_2$ can be calculated according to Wei et al. [23] formula:

$$E_g(x) = (1-x)E_g^{CIS} + xE_g^{CGS} - bx(1-x) \quad (5)$$

Where x is the ratio of Ga/ (In + Ga) and the bowing coefficient, b is about 0.21 eV. In case of Ga/(In + Ga) = 0.3 as in our CIGS sample E_g = 1.13 eV which is in good agreement with the value extrapolated.

Similar values of the bandgap are also found by Siebentritt et al. [24] and Theodoropoulou et al. [18] for CIS and CIGS, respectively.

Fig. 5 depicts a PL spectrum of CIGS thin films of various compositions in the temperature range 20–200 K. No emission at all the high-energy part (close to the bandgap) was observed in most of the samples. Whenever the signal close to bandgap was observed, it consisted of broad overlapping peaks. One example is shown in Fig. 5(a) for CIS sample. According to Siebentritt et al. [24], its shape and position are typical for Cu-poor CIS, while the signal intensity is very low comparing to typical emission measured in CIGS films produced by standard co-evaporation methods [8]. A feature characteristic for PL spectra of our samples is the presence of the low energy, defect-related signals. It is dominating the spectrum for all samples, and in most of them, it is the only one detected. E.g. in case of CGS sample, a very prominent peak around 1 eV is observed while no emission in the vicinity of the bandgap was detected at all.

More detailed typical peak analyses of the PL spectra are depicted in the insets of Fig. 5. The insets show the experimental data (orange line) and the results of fitting to Gaussian distribution (dash lines) at T = 20 K. In case of the CIS spectrum, the de-convolution of two peaks appearing close to the bandgap provided values of 0.948 eV and 0.978 eV. These emissions were usually attributed to either to a free-bound (FB) or a donor–acceptor (DA) transition. Siebentritt [24] showed that the exact position of these signals labeled here as P2 and P3 depended on the deviation from stoichiometry - the shift towards lower energies and broadening of the spectrum increases with copper deficiency was observed and attributed to an increase of fluctuating electrostatic potentials. The low energy emission P1 was too close to the spectral limit of Ge detector which made the de-convolution not possible. This peak was assigned to the donor–acceptor pairs (DAP) transition [25].

In the CIGS thin film with 30% of gallium that low energy emission moved towards higher energy, therefore we were able to perform the de-convolution of these signals. The analysis provided peak values (inset of Fig. 5(b)), equal to 0.718 eV, 0.73 eV, and 0.761 eV. These peaks were assigned to DAP transition. Typical PL emissions around 0.95 eV and 1 eV and attributed to free-to-bound transitions (FB) involving InCu antisite or Cu vacancy (In_{Cu} and V_{Cu}) [26–29] were not observed in our sample.

The PL spectra of CGS are displayed in Fig. 5(c). Peaks at around 0.827 eV and 0.981 were observed, no emission involving shallow defects was detected. The emission from deep defects at somewhat higher energies (1.10 eV and 1.24 eV) was observed also in the epitaxial Cu-rich CGS samples by Spindler et al. [30]. It was attributed to deep donor-acceptor transitions involving one acceptor and two different donor states. According to Spindler et al. [30], these deep donors were attributed to two antisite defect states, Ga_{Cu} and Ga_{Cu}^{2-}. These two deep broad transitions were observed in our sample near 0.827 eV (DDA_1) and 0.981 eV (DDA_2) and it was fitted with Gaussian distributions with FWHM values of 192 meV and 202 meV, respectively as it is shown in the inset of Fig. 5(c).

It is worth to note that very deep PL emissions move towards lower energies with decreasing gallium content in our samples: peak below 0.7 eV in CIS, 0.72–0.76 eV in CIGS and 0.82–0.98 in CGS.

For more quantitative analyses, the temperature dependency of the emission magnitudes is depicted in Fig. 6 where we use the following Boltzmann distribution function:

$$1/1 + T^{3/2}\sum_{i=1} a_i e^{-E_{ai}/k_B T}.$$

Here E_a is the carrier activation energy, k_B is the Boltzmann constant, and T is temperature. The PL intensity at high temperatures is then given by the following formula:

$$I(E) \propto \ exp(-E_a/k_B T) \quad (6)$$

Fig. 6 depicts the PL temperature dependence in the temperature range of 20–160 K for CIGS thin films of various compositions. The total peak intensity evaluated by integration of the peaks P1 in case of CIS, P2 in case of CIGS and P2 for CGS. At $T < 60$ K, the line shape remains constant and broader at the low energy part. At $T \geq 60$ K, the curves start to drop slightly and tend to follow a straight line in the semi-logarithmic scale. In this range, the PL spectra exhibit an important broadening of the high energy part. These features imply that at $T > 60$ K the carriers have attained thermal equilibrium while at $T < 60$ K the carriers are not thermalized.

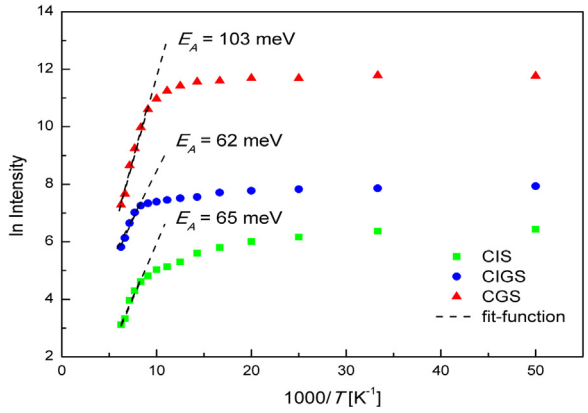

Fig. 6. Logarithm of the peak area versus reciprocal temperature for all CIGS composition samples. Linear fits at high temperature are shown (straight lines) with the activation energies.

The activation energies were extracted from the linear fits of the high-temperature slope and they are lower than found in [24,30]. We attribute these differences to much more defected CGS material with more pronounced potential fluctuations than epitaxial samples investigated in [24].

4. Conclusion

CIGS layers on SnO_2 substrates grown by CSVT technique were investigated by several structural and optical methods. XRD analysis revealed the chalcopyrite structure of CIGS with a (112) dominant peak. The decrease in lattice constants has been observed with the increase in Ga concentration. The Raman studies indicate the shift in peak towards higher value with the increase in Ga content and allow detecting the presence of Cu_2Se secondary phase in CGS sample. The bandgap energy of the investigated samples is around 0.98, 1.12 and 1.57 eV for CIS, CIGS, and CGS, respectively. They are shifted towards lower energies comparing to literature data [14,21,22] indicating defect-related broadening of the bands, especially in case of CGS sample. The most important feature of the PL study was the observation of emission related to DAP process prevailing over typical free-to-bound transitions observed at low temperatures in CIGS compounds. It is a sign of exceptionally large concentration of deep defects in the studied materials.

Summing up, the results of XRD and Raman measurements confirm good crystalline and compositional quality of the CIS and CIGS samples obtained by CSVT. Only in the CGS layer, a contribution of secondary phase Cu_2Se was detected. However, photoluminescence intensity is much weaker in all samples than in case of absorbers used in the efficient CIGS devices [8,31] indicating a domination of non-radiative transitions. The spectra feature rather an emission from very deep levels while typical transitions involving shallow states are practically absent. We conclude that the films obtained by CSVT are much more defected and its optoelectronic properties are worse compared to the CIGS polycrystalline thin films fabricated by co-evaporation.

Acknowledgements

The authors would like to acknowledge the team of Warsaw University of Technology, Faculty of Physics, and in particular dr A. Urbaniak and dr J. Antonowicz for their help in the experiments.

H. Tassoult is also thankful to C. Spindler from Laboratory for Photovoltaics, Physics and Material Science Research Unit, University of Luxembourg, for his scientific help.

References

[1] P. Jackson, D. Hariskos, R. Wuerz, O. Kiowski, A. Bauer, T.M. Friedlmeier, M. Powalla, Properties of Cu(In,Ga)Se_2 solar cells with new record efficiencies up to 21. 7%, Phys. Status Solidi 4 (2014) 28–31.

[2] K. Rui, Y. Takeshi, A. Shunsuke, H. Atsushi, F. T. Kong, K. Takuya, and S. Hiroki, "New World Record Cu(In,Ga)(Se,S)$_2$ Thin Film Solar Cell Efficiency Beyond 22%," in: Proceedings of the IEEE 43rd Photovolt. Spec. Conf. , 2016, pp. 1287–1291.

[3] M. Nouiri, K. Djessas, L. El Mir, J.L. Gauffier, S. Alaya, Effect of the growth temperature on the structural, morphological and electrical properties of $CuIn_{0.7}Ga_{0.3}Se_2$ layers grown by CSVT technique, Thin Solid Films 516 (20) (2008) 7088–7093.

[4] M. Nouiri, Z. Ben Ayadi, K. Khirouni, S. Alaya, K. Djessas, S. Yapi, Effect of substrate temperature and source grain size on the structural and electrical properties of CSVT grown Cu($In_{1-x}Ga_x$)Se_2 thin films (SPEC. ISS.), Mater. Sci. Eng. C 27 (5–8) (2007) 1002–1006.

[5] G. Massé, K. Djessas, C. Monty, F. Sibieude, Morphology of Cu(In,Ga)Se_2 thin films grown by close-spaced vapor transport from sources with different grain sizes, Thin Solid Films 414 (2002) 192–198.

[6] C. Insignares-Cuello, V. Izquierdo-Roca, J. López-García, L. Calvo-Barrio, E. Saucedo, S. Kretzschmar, T. Unold, C. Broussillou, T. Goislard de Monsabert, V. Bermudez, A. Pérez-Rodríguez, Combined Raman scattering/photoluminescence analysis of Cu(In,Ga)Se_2 electrodeposited layers, Sol. Energy 103 (2014) 89–95.

[7] A. Bouloufa, K. Djessas, D. Todorovic, Structural and optical properties of Cu(In,Ga)Se_2 grown by close-spaced vapor transport technique, Mater. Sci. Semicond. Process. 12 (1–2) (2009) 82–87.

[8] M. Pawlowski, P. Zabierowski, R. Bacewicz, H. Marko, N. Barreau, Photoluminescence as a tool for investigations of the junction region in Cu(In,Ga)Se_2-based solar cells, Thin Solid Films 519 (21) (2011) 7328–7331.

[9] J. Olejníček, C.A. Kamler, A. Mirasano, A.L. Martinez-Skinner, M.A. Ingersoll, C.L. Exstrom, S.A. Darveau, J.L. Huguenin-Love, M. Diaz, N.J. Ianno, R.J. Soukup, A non-vacuum process for preparing nanocrystalline $CuIn_{1-x}Ga_xSe_2$ materials involving an open-air solvothermal reaction, Sol. Energy Mater. Sol. Cells 94 (1) (2010) 8–11.

[10] B. Vidhya, S. Velumani, J.A. Arenas-Alatorre, A. Morales-Acevedo, R. Asomoza, J.A. Chavez-Carvayar, Structural studies of mechano-chemically synthesized $CuIn_{1-x}Ga_xSe_2$ nanoparticles, Mater. Sci. Eng. B Solid-State Mater. Adv. Technol. 174 (1–3) (2010) 216–221.

[11] A. Ben Marai, J. Ben Belgacem, Z. Ben Ayadi, K. Djessas, S. Alaya, Structural and optical properties of $CuIn_{1-x}Ga_xSe_2$ nanoparticles synthesized by solvothermal route, J. Alloy. Compd. 658 (2015) 961–966.

[12] A. Urbaniak, M. Pawłowski, M. Marzantowicz, T. Sall, B. Marí, Opto-electrical characterisation of In-doped SnS thin films for photovoltaic applications, Thin Solid Films 636 (2017) 158–163.

[13] J. Claypoole, B. Peace, N. Sun, D. Dwyer, M.D. Eisaman, P. Haldar, H. Efstathiadis, Characterization of Cu(In,Ga)Se_2 (CIGS) films with varying gallium ratios, J. Alloys Compd., 2015.

[14] W. Witte, D. Abou-Ras, K. Albe, G.H. Bauer, F. Bertram, C. Boit, R. Brüggemann, J. Christen, J. Dietrich, A. Eicke, D. Hariskos, M. Maiberg, R. Mainz, M. Meessen, M. Müller, O. Neumann, T. Orgis, S. Paetel, J. Pohl, H. Rodriguez-Alvarez, R. Scheer, H.W. Schock, T. Unold, A. Weber, M. Powalla, Gallium gradients in Cu(In,Ga)Se_2 thin-film solar cells, Prog. Photovolt. (2014).

[15] V. Izquierdo-Roca, X. Fontané, E. Saucedo Silva, J.S. Jaime-Ferrer, J. Alvarez-Garcia, A. Pérez-Rodríguez, V. Bermúdez Benito, J.R.J.R. Morante, J. Álvarez-García, A. Pérez-Rodríguez, Process monitoring of chalcopyrite photovoltaic technologies by Raman spectroscopy: an application to low cost electrodeposition based processes, New J. Chem. 35 (2) (2011) 453–460.

[16] X. Fontané, V. Izquierdo-Roca, L. Calvo-Barrio, A. Prez-Rodríguez, J.R. Morante, D. Guettler, A. Eicke, A.N. Tiwari, Investigation of compositional inhomogeneities in complex polycrystalline Cu(In,Ga)Se_2 layers for solar cells, Appl. Phys. Lett. 95 (26) (2009).

[17] Y. Liu, D. Kong, J. Li, C. Zhao, C. Chen, J. Brugger, Preparation of Cu(In,Ga)Se_2 thin film by solvothermal and spin-coating process, Energy Procedia 16 (2012) 217–222.

[18] S. Theodoropoulou, D. Papadimitriou, N. Rega, S. Siebentritt, M.C. Lux-steiner, Raman and photoreflectance study of $CuIn_{1-x}Ga_xSe_2$ epitaxial layers, Thin Solid Films 512 (2006) 690–694.

[19] V. Izquierdo-Roca, A. Prez-Rodríguez, A. Romano-Rodríguez, J.R. Morante, J. Álvarez-García, L. Calvo-Barrio, V. Bermudez, P.P. Grand, O. Ramdani, L. Parissi, O. Kerrec, Raman microprobe characterization of electrodeposited S-rich CuIn(S,Se)$_2$ for photovoltaic applications: microstructural analysis, J. Appl. Phys. 101 (10) (2007).

[20] A. Cho, S. Ahn, J.H. Yun, J. Gwak, S.K. Ahn, K. Shin, J. Yoo, H. Song, K. Yoon, The growth of $Cu_{2-x}Se$ thin films using nanoparticles, Thin Solid Films 546 (2013) 299–307.

[21] W. Witte, R. Kniese, M. Powalla, Raman investigations of Cu(In,Ga)Se_2 thin films with various copper contents, Thin Solid Films 517 (2) (2008) 867–869.

[22] M.A. Contreras, K. Ramanathan, J. Abushama, F. Hasoon, D.L. Young, B. Egaas, R. Noufi, Diode characteristics in state of the art ZnO/CdS/ Cu($In_{1-x}Ga_x$)Se_2 solar cells, Prog. Photovolt. Res. Appl. 13 (3) (2005) 209–216.

[23] S.H. Wei, S.B. Zhang, A. Zunger, Effects of Ga addition to $CuInSe_2$ on its electronic, structural, and defect properties, Appl. Phys. Lett. 72 (24) (1998) 3199–3201.

[24] S. Siebentritt, N. Rega, A. Zajogin, M.C. Lux-Steiner, Do we really need another PL study of $CuInSe_2$? Phys. Stat. Sol. C. Conf. 1 (9) (2004) 2304–2310.

[25] K. Topper, J. Bruns, R. Scheer, M. Weber, A. Weidinger, D. Braunig, Photoluminescence of $CuInS_2$ thin films and solar cells modified by postdeposition

treatments, Appl. Phys. Lett. 71 (482) (1997).
[26] J. Parravicini, M. Acciarri, M. Murabito, A.L. Donne, A. Gasparotto, S. Binetti, In-depth photoluminescence spectra of pure CIGS thin films, Appl. Opt. 57 (2018) 1849.
[27] J. Yang, H.W. Du, Y. Li, M. Gao, Y.Z. Wan, F. Xu, Z.Q. Ma, Structural defects and recombination behavior of excited carriers in Cu(In,Ga)Se_2 solar cells, AIP Adv. 6 (2016) 085215.
[28] S. Shirakata, T. Nakada, Photoluminescence and time-resolved photoluminescence in Cu(In,Ga)Se_2 thin films and solar cells, Phys. Stat. Sol. C 6 (5) (2009) 1059–1062.
[29] Y. Liao, Y.K. Liao, S.Y. Kuo, W.T. Lin, F.I. Lai, D.H. Hsieh, M.A. Tsai, S.C. Chen, D.W. Chiou, J.C. Chang, K.H. Wu, S.J. Cheng, H.C. Kuo, Observation of unusual optical transitions in thin-film Cu(In,Ga)Se_2 solar cells, Opt. Express 20 (2012) 838–842.
[30] C. Spindler, D. Regesch, S. Siebentritt, Revisiting radiative deep-level transitions in $CuGaSe_2$ by photoluminescence, Appl. Phys. Lett. 109 (3) (2016).
[31] M. Pawłowski, P. Zabierowski, R. Bacewicz, N. Barreau, Influence of Ga-notch position on recombination processes in Cu(In,Ga)Se_2 -based solar cells investigated by means of photoluminescence, Thin Solid Films 535 (2013) 336–339.